Packet-Pair Sizing for Controlling Packet Dispersion on Wired Heterogeneous Networks

Khondaker M. Salehin and Roberto Rojas-Cessa
Networking Research Laboratory, ECE Department
New Jersey Institute of Technology, Newark, NJ 07102–1982
Email: {kms29, rojas}@njit.edu

***Abstract*—The packet-pair structure is a widely used probing technique for measuring link capacity over network paths. In packet-pair probing, the probe-gap value at the link of interest (e.g., the link with the smallest capacity or any link along a path) is determined for link-capacity measurement, which can be affected if dispersion (i.e., separation) of the packet pair is created by the heterogeneous link capacities and cross traffic over an end-to-end path. In this paper, we present an analytical model concerning the effect of heterogeneous link capacities and cross traffic on the packet-pair structure over a multiple-hop path, and define the constraints on the packet sizing for accurate end-link (i.e., the link connected to the destination node of an end-to-end path) capacity measurement. We test the model through numerical evaluations and experimentally, on end-to-end paths with heterogeneous links and different cross traffic loads. The experiments are performed on a testbed and in the Internet.**

***Index Terms*—Active probing, packet pair, packet sizing, link capacity, analytical model.**

I. Introduction

Packet-pair structure is a widely used probing technique for measuring link capacity of network paths [1]–[6]. In packet-pair probing, two packets are sent from the source node to the destination node of an end-to-end path to measure the probe gap of the packet pair at the link of interest (e.g., the narrow link, the smallest link capacity, or any link along the path) for capacity measurement. The accuracy of link-capacity measurement based on the probe gap can be affected if additional dispersion (i.e., separation) in the packet-pair structure is created by the heterogeneous link capacities and cross traffic of the path [4].

The sizes of probing packets in the packet-pair structure is an important parameter for link-capacity measurement, and the effect of link heterogeneity and cross traffic on the measurement accuracy can be reduced if suitable packet sizes are used over a path [2]–[4]. In this paper, we present an analytical model concerning the effect of heterogeneous link capacities and cross traffic on the packet-pair structure as it travels over a multiple-hop path and define the constraints on the packet sizing for accurate end-link (i.e., the link connected to the destination node of an end-to-end path) capacity measurement.

The remainder of the paper is organized as follows: In Section II, we discuss existing link-capacity measurement schemes. In Section III, we present a packet-pair structure. In Section IV, we present an analytical model for sizing the probing packets in the packet-pair structure and verify the model through numerical evaluations. In Section V, we show experimental results of end-link capacity measurement over testbed and Internet paths. In Section VI, we conclude the discussion.

II. Related Work

A plethora of packet-pair based schemes to measure link capacity have been proposed [1]–[6]. Because we aim to estimate the end-link capacity of a path in this paper, we limit the discussion to two prominent per-hop measurement schemes, which measures the capacities of all links along a path, that may be applicable to that case.

Nettimer is an early per-hop scheme to measure link capacities of an end-to-end path based on tailgating technique, where a small packet tailgating a large packet is sent back-to-back from the source node to the destination node [2]. The one way delay (OWD) of the small packet in the packet pair is used for capacity estimation. In the tailgating technique, the large packet is dropped right before reaching the link of interest and the small packet is left to continue toward the destination node to identify the contribution to OWD of the link of interest. Although the probe gap of the packet-pair structure is not considered in Nettimer, this scheme requires that the packet pair hold a zero-dispersion gap before arriving at the link of interest to avoid measurement error due to link heterogeneity and cross traffic over the path. However, it is unclear whether a packet pair could keep a zero-dispersion gap throughout the path as no analytical model was presented. The reported implementation of Nettimer shows around 50% measurement accuracy [2].

Different from the traditional per-hop scheme approach, Cartouche probing measures the capacities of target links in a segment of a path under interest [5]. This scheme sends a train of probing packets in pairs, where each pair consists of a large packet tailgated by a small packet, similar to the single packet pair in Nettimer. All the packets in the probing train are dropped before reaching the link of interest while the small packets of the first and last packet pairs reach the destination node. The scheme measures the gap between the small packets at the destination node for capacity estimation. The accuracy of the scheme depends on the size of the probing train (i.e., number of packet pairs), which depends on the ratios of the link capacities along the path. It is reported that the scheme has been tested under low cross-traffic loads [5].

III. Compound Probe

Figure 1 shows a packet-pair structure comprising two probing packets: a heading packet (P_h) followed by a trailing packet (P_t) [2], and we call this a compound probe [7], [8]. The sizes of P_h and P_t are denoted as s_h and s_t, respectively. The gap in between the last bit of P_h and the last bit of

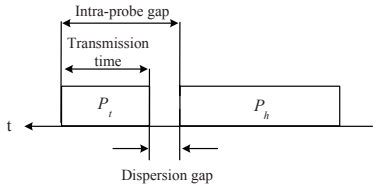

Fig. 1. Compound-probe structure.

P_t is called the *intra-probe gap*, $G(s_t)$, which includes the transmission time of P_t.

The two probing packets in the compound probe are used to identify the beginning and the end of P_t (i.e., the transmission time of the trailing packet) as the time-stamping process records the arrival time at which a packet has been received successfully. To determine the transmission time of P_t on the end link of a path from $G(s_t)$, the dispersion gap between P_h and P_t (i.e., the separation between the last bit of P_h and the first bit of P_t) is required to be zero at the time of arrival in the destination node.

In a compound probe, gap dispersion (i.e., the increment of the dispersion gap) can occur if one or two of the following events occur: 1) if the packet-size ratio of the compound probe, $\alpha = \frac{s_h}{s_t}$, is smaller than the link-capacity ratio of the input and output links of a network node i, $lr_i = \frac{l_{i+1}}{l_i}$, or 2) one or more cross-traffic packets are enclosed between P_h and P_t. Because event 2 is out of our reach, we mainly focus on event 1. According to event 1, if the transmission time of P_h at the output link is smaller than the transmission of P_t at the input link of a network node, the compound probe experiences dispersion [2], [5]. Therefore, at the network node i, the packet-size ratio α between P_h and P_t to avoid gap dispersion must follow

$$\alpha \geq \frac{l_{i+1}}{l_i}. \tag{1}$$

For end-link capacity measurement, a zero-dispersion gap is required at the end link of the followed path. This requirement can be achieved even if a dispersion gap is created along the path but it becomes zero before reaching the end link (e.g., due to a link-capacity ratio smaller than 1). To avoid uncertainty, a model to ensure the above requirement considering the link heterogeneity and cross traffic of the path is required.

IV. Sizing of Probing Packets

In this section, we present an analytical model for sizing P_h and P_t to ensure a zero-dispersion gap on the end link of a path considering the effects of link heterogeneity and cross traffic on intermediate links. Different from [2], our model considers cross traffic and an end-to-end path.

A. Sizing of Probing Packets and Link Heterogeneity

Consider that the link capacities between node 0 (src) and node n (dst) along a n-hop path are l_1, ..., l_n, as shown in Figure 2. To keep a zero-dispersion gap between P_h and P_t at dst, the following equation applies:

$$(\frac{s_h}{l_n} - \frac{s_h}{\alpha l_{n-1}}) + (\frac{s_h}{l_{n-1}} - \frac{s_h}{\alpha l_{n-2}}) + ... + (\frac{s_h}{l_{z+1}} - \frac{s_h}{\alpha l_z}) = 0 \tag{2}$$

where $\frac{s_h}{\alpha} = s_t$, and l_z is the capacity of a link connected to a node z, such that $lr_z = \frac{l_{z+1}}{l_z}$ is the largest link-capacity ratio along the path, located after the narrow link (in the direction from src to dst) and that l_z also is the link closest to dst (e.g., if two nodes following the narrow link closest to dst of the path have the largest link-capacity ratio, the node located the closest to dst is selected). Therefore, the index z is such that $1 \leq z \leq (n-1)$. Equation (2) is valid as long as the narrow link is not the end link of the path.

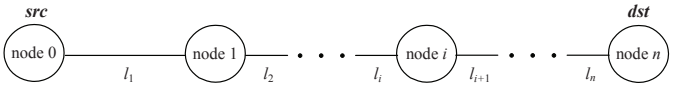

Fig. 2. n-hop end-to-end path.

The largest size of P_t is calculated from (2) as:

$$s_t = s_h \frac{\sum_{j=z+1}^{n} \frac{1}{l_j}}{\sum_{j=z}^{n-1} \frac{1}{l_j}} \tag{3}$$

When the end-link capacity l_n is the path's narrow link, the required condition to achieve a zero-dispersion gap is:

$$\frac{s_h}{l_n} - \frac{s_h}{\alpha l_{n-1}} = 0 \tag{4}$$

and the largest size of P_t is calculated as:

$$s_t = \frac{s_h}{l_n} l_{n-1} \tag{5}$$

The rationale behind (2) and (4) is that a compound probe may experience the largest dispersion at a network node over a path where the link-capacity ratio is the largest and the packet-size ratio is smaller than the largest link-capacity ratio. Therefore, s_t is determined with respect to s_h by finding a suitable packet-size ratio so that the dispersion gap reduces to zero upon arriving at node n.

B. Sizing of Probing Packet and Cross-Traffic Effect

Figure 3 shows an example of a compound probe forwarded from the input link to the output link by node i when two cross-traffic packets, denoted by D_h and D_t, intrude the compound probe. The capacity of the input and output links are l_i and l_{i+1}, respectively, where $l_i < l_{i+1}$ in this example. Here, P_h and P_t arrive at node i with a zero-dispersion gap. However, the compound probe experiences dispersion at the output link, as shown by the dispersion gap in the figure.

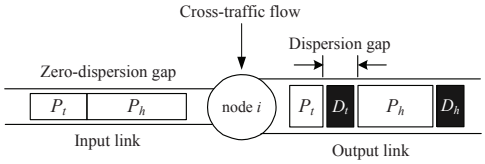

Fig. 3. Forwarding of a compound probe by node i from its input link to its output link.

The intra-probe gap of the compound probe at the output link of node i is defined as:

$$G(s_t)_{i+1} = \frac{s_t}{l_{i+1}} + \delta_{i+1}, \quad (6)$$

where the dispersion gap at the output link, δ_{i+1}, is:

$$\delta_{i+1} = \begin{cases} \delta_i - \Delta tr(h,t)_i & \text{if } \delta_i - \Delta tr(h,t)_i > Qt_i \\ Qt_i & \text{else} \end{cases} \quad (7)$$

In the above equation, δ_i is the dispersion gap at the input link of node i, $\Delta tr(h,t)_i$ is the difference between the transmission time of P_h plus the queuing delay (Qh_i) caused by the cross-traffic packet(s) backlogged ahead of P_h at the output link and the transmission time of P_t at the input link of node i. Qt_i is the increment of the dispersion gap caused by the cross-traffic packet(s) inserted between P_h and P_t at node i. These terms are estimated as:

$$\Delta tr(h,t)_i = \frac{s_h}{l_{i+1}} + Qh_i - \frac{s_t}{l_i} \quad (8)$$

$$Qh_i = \sum_u \frac{\zeta_{u(i)}}{l_{i+1}};\ u \geq 0 \quad (9)$$

$$Qt_i = \sum_v \frac{\zeta_{v(i)}}{l_{i+1}};\ v \geq 0 \quad (10)$$

Here, $\zeta_{u(i)}$ and $\zeta_{v(i)}$ denote the sizes of the cross-traffic packets u and v ahead of P_h and P_t for Qh_i and Qt_i, respectively, at node i.

When node n of Figure 2 measures the intra-probe gap of the compound probe upon receiving it at the application layer, the measured intra-probe gap includes the interframe gap (IFG) [9] of the end link and it follows (6):

$$G(s_t)_n = \frac{s_t}{l_n} + \delta_n + IFG \quad (11)$$

C. Numerical Evaluations of Packet-Sizing Model

We calculated the upper bounds of α (i.e., the largest possible values of s_t against s_h) needed to keep the dispersion gap at zero using (3) or (5) over a four-hop end-to-end path, considering different configurations for the link capacities, as shown in Table I. The four different configurations, each denoted as Cc-R where c is the identification index for each of the four considered configurations and R is the capacity of the end link of configuration c, are C1-10, C2-100, C3-100, and C4-100. These configurations provide diversity of the link capacity assignments and the location of narrow link in each configuration is also different.

TABLE I
TESTBED PATH CONFIGURATIONS AND ESTIMATED PACKET-SIZE RATIOS

Path	Link capacity (l_i) (Mb/s)				Link-capacity ratio ($lr_i = \frac{l_{i+1}}{l_i}$)			Packet-size ratio ($\alpha = \frac{s_h}{s_t}$)	
	l_1	l_2	l_3	l_4	lr_1	lr_2	lr_3	Calculated	Evaluated
C1-10	100	155	100	10	1.55	0.645	0.1	1	1
C2-100	10	155	10	100	15.5	0.064	10	10	10
C3-100	100	10	155	100	0.1	15.5	0.645	6.49	6.67
C4-100	10	10	155	100	1	15.5	0.645	6.49	6.67

To verify the calculated values, we evaluated the values of α using the dispersion-gap model in Section IV-B, considering Qt_i and Qh_i equal to zero in (7) and (8). To evaluate with different αs, the initial value of s_t is set to 50 bytes and it is gradually increased by 25 bytes until the length of s_h = 1500 bytes is reached. The last two columns of Table I show the lower bounds of both the calculated and evaluated values of α for each configuration. Here, both the calculated and evaluated values were obtained by using a single compound-probe over each path configuration. According to Table I, the evaluated values are very close to the calculated ones; the calculated values of α over C1-10 to C4-100 are 1 (s_t = 1500 bytes), 10 (s_t = 150 bytes), 6.49 (s_t = 232 bytes), and 6.49 (s_t = 232 bytes), respectively. The evaluated values of α are 1 (s_t = 1500 bytes), 10 (s_t = 150 bytes), 6.67 (s_t = 225 bytes), and 6.67 (s_t = 225 bytes) over C1-10, C2-100, C3-100, and C4-100, respectively. The small over estimation in the evaluated values for C3-100 and C4-100 are produced by the 25-byte step increase of s_t, as stated above.

Figures 4(a)-4(d) show detailed information about the estimated end-link capacities over each path configuration using different values of α, after considering $IFG = 0$ in (11). The acceptable packet-size ratios are those representing the actual end-link capacity, as indicated by the arrows in the figures (where the zero-dispersion gap can be kept).

D. Impact of Cross Traffic on Packet-Size Ratio

The impact of cross traffic in the measurement of end-link capacity was evaluated considering a symmetric cross-traffic load over the second and third links of each path configurations. In this evaluation, we considered the same values of α, as used in Section IV-C, along with three different values for u and v, i.e., 1, 5, and 10 packets, each packet is 64 bytes, in (9) and (10). Figures 4(e)-4(h) show the estimated end-link capacities over C1-10 to C4-100, respectively. The estimated end-link capacities show that the cross-traffic interference increases the upper bounds of α for accurate link-capacity measurement except over C1-10, where the end link is the narrow link of the path. For example, when P_h and P_t of the compound probe is interfered by a single cross-traffic packet (i.e., when $u = 1$ and $v = 1$), the upper bound of α increases from 10 to 20 (i.e., s_t decreases to 75 bytes) over C2-100, and from 6.67 to 8.57 (i.e., s_t decreases to 175 bytes) over both C3-100 and C4-100, according to Figures 4(f)-4(h), respectively. Here, we can see that if the narrow link is other than the end link, cross traffic produces dispersion. Another observation is that a large α simplifies the selection of the sizes of P_h and P_t. In this case, the largest value of α achievable on Ethernet is sufficient to achieve a zero-dispersion gap in the considered path configurations.

V. Experimental Results

We tested the above analytical model to measure end-link capacity over testbed and Internet paths. We used Linux based commodity workstations as src and dst in the experimental paths. The specification of the workstation at dst is shown in Table II.

A. Experimental Measurement on a Controlled Testbed

In the testbed experiment, we considered the first two path configurations, C1-10 and C2-100, of Table I because they have the smallest and the largest upper-bound values of α, respectively, among the four listed path configurations. We

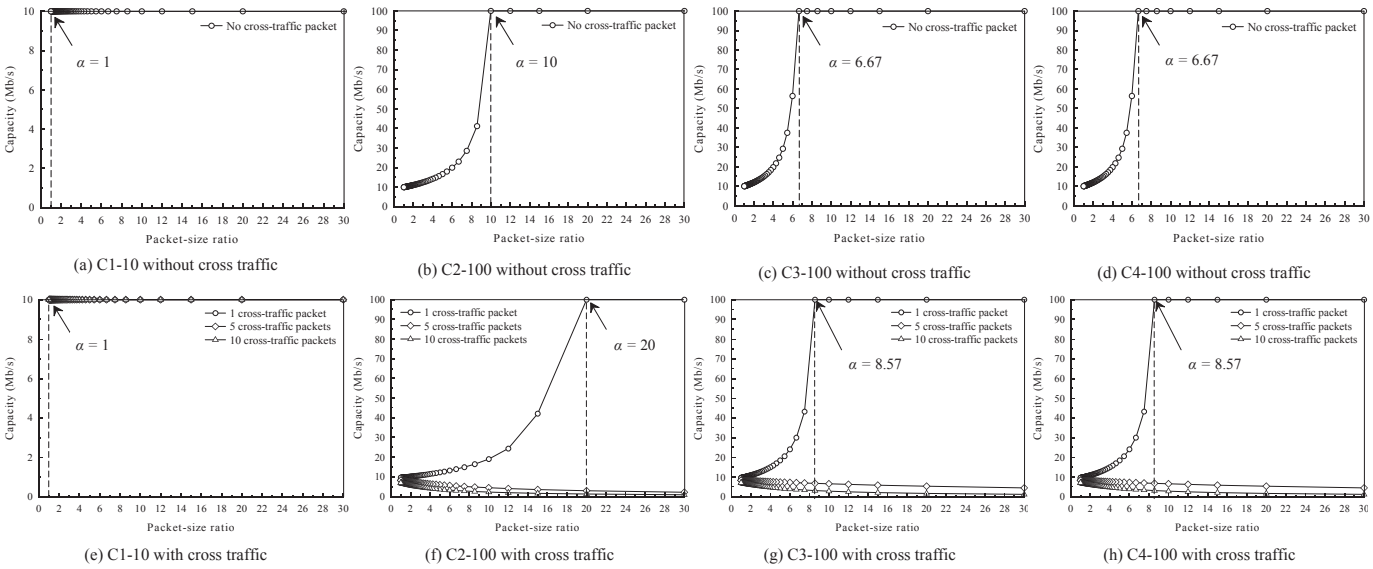

Fig. 4. Evaluation of packet-size ratio (α) to measure the end-link capacity (l_4) of four different path configurations: (a) C1-10, (b) C2-100, (c) C3-100, and (d) C4-100 without cross-traffic load. (e) C1-10, (f) C2-100, (g) C3-100, and (h) C4-100 with cross-traffic load.

TABLE II
SPECIFICATIONS OF THE WORKSTATION AT dst

	Dell Inspiron 531S
Name	I531S
Processor (CPU speed)	AMD Athlon 64 X2 Dual Core (1 GHz)
RAM size	1024 MB
RAM speed (data width)	667 MHz (64 bits)
PCI bus speed	133 MB/s
Interface speed	10/100 Mb/s
Linux kernel version	2.6.18

implemented these two paths on a testbed consisting of three Cisco routers, as intermediate nodes, and two Linux workstations, as src and dst (see Table II for the specifications). We also implemented a compound-probe based probing tool as an application on Linux system, which provides a clock with 1-μs resolution for time stamping (based on the pcap library [10]). For end-link capacity measurement, we used two compound probes over each path having a common s_h and two different s_ts to test our analytical model. The value of s_h was determined by the maximum transmission unit (MTU) over each path: 1448 bytes of user datagram protocol (UDP) payload plus 54 bytes of Ethernet encapsulation at the end link (Ethernet encapsulation includes a 12-byte preamble, start of frame delimiter, SFD, and frame check sequence, FCS, fields). The values of s_t used in the two compound probes are 87 bytes and 112 bytes, respectively, since these values provide two large packet-size ratios (e.g., $\alpha_1 = \frac{1502\ bytes}{87\ bytes} = 17.26$ and $\alpha_2 = \frac{1502\ bytes}{112\ bytes} = 13.41$) which ensure a zero-dispersion gap at dst over each testbed path configuration. Moreover, these values are within the upper bounds of the packet-size ratios of both C1-10 and C2-100. We sent 500 compound-probes using each s_t size to measure the end-link capacity. The time stamps of each compound probe at dst were obtained using Wireshark [11].

1) Measured Intra-Probe Gaps at dst. Figure 5 shows the distributions of the intra-probe gaps measured by dst over each testbed path when there was no cross-traffic load. The theoretical values of the intra-probe gaps on the end link, i.e., the value of $G(s_t)_n$ when δ_n = 0 in (11), for the 87- and 112-byte trailing packets over C1-10 are 80 and 100 μs, respectively, considering $IFG = 9.6$ μs for l_4 = 10 Mb/s [9]. The theoretical intra-probe gap values for the same packet sizes over C2-100 are 8 and 10 μs, respectively, considering $IFG = 0.96$ μs for l_4 = 100 Mb/s [9]. According to Figure 5(a), the intra-probe gaps measured over C1-10 for the 87- and 112-byte packets are tightly clustered around 79 and 99 μs, respectively. Over C2-100, the measured intra-probe gaps are clustered around 7 and 9 μs for the respective packet sizes, as shown by Figure 5(b). The solid and a dashed vertical-lines indicate the theoretical values and G_{peak} indicates the most frequent intra-probe gap for the 87- and 112-byte packets, respectively, in both graphs. In each graph, the measured intra-probe gaps smaller than the theoretical values are due to the 1-μs clock resolution in the Linux system [12], [13]. However, the measured intra-probe gaps show that the compound probes did not experience dispersion over the paths since the used packet-size ratios avoid the effect of link heterogeneity.

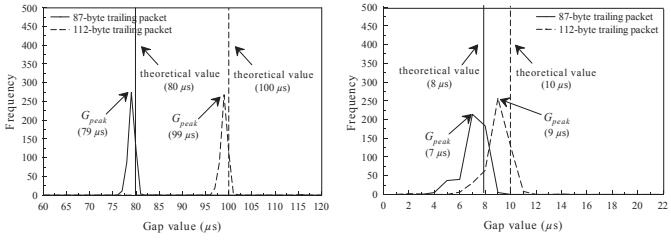

Fig. 5. Distributions of intra-probe gaps measured at dst over (a) C1-10 and (b) C2-100 without cross-traffic load.

2) Effect of Cross Traffic on Intra-probe Gap Measurement. Figure 6 shows the measured intra-probe gaps over C1-10 and C2-100 with 60% cross-traffic load, which consists of two symmetric cross-traffic flows at the second and third links,

respectively, of each four-hop path. We used small packet sizes, between 64 and 128 bytes, and the constant-bit-rate (CBR) traffic model in each flow to create a demanding environment on the testbed paths. In Figure 6, the distributions of the intra-probe gaps are similar to those in Figure 5 and the majority of the compound probe arrives at dst with a zero-dispersion gap for both trailing packet sizes. However, Figure 6(b) has some outlier values (i.e., large intra-probe gaps) at the right-hand side of the graph for both packet sizes, as compared to Figure 5(b). These gaps are affected by cross traffic which corresponds to the scenario when $\delta_n > 0$ in (11).

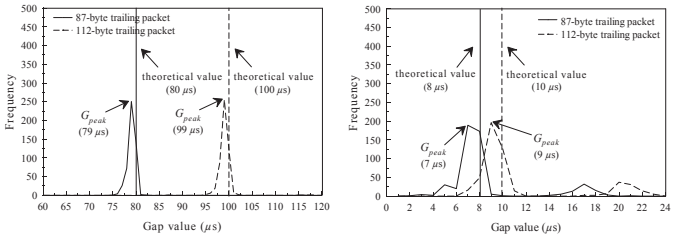

(a) C1-10 with 60% cross traffic (b) C2-100 with 60% cross traffic

Fig. 6. Distributions of intra-probe gaps measured at dst over (a) C1-10 and (b) C2-100 with 60% cross-traffic load.

B. Experimental Measurements in the Internet

We tested our analytical model over two Internet paths, an inter-state path in the U.S. and an international path between Taiwan and the U.S., between December 2010 and January 2011. The inter-state path was set between New York Institute of Technology (NYIT), New York, New York and New Jersey Institute of Technology (NJIT), Newark, New Jersey. This path is labeled as NYNJ and comprises 19 hops. The international path was set between Chaoyang University of Technology (CYUT), Taichung, Taiwan, and NJIT. This path is labeled as TWNJ and comprises 21 hops. We configured the workstations at NYIT and CYUT as src and the workstation (I531S) at NJIT as dst. These workstations were connected to either 10-Mb/s or 100-Mb/s links, but the capacities of the intermediate links along the paths are unknown. As for measuring the end link, the same s_t values used on the tested paths, 87 and 112 bytes, were considered. However, s_h = 1512 bytes was used instead of 1502 bytes considering the maximum payload size in an IP packet. We also used 500 compound-probes of each s_t size over each path, as in the testbed experiment. Figures 7(a) and 7(b) show the distributions of the intra-probe gaps measured by dst connected to 10-Mb/s and 100-Mb/s links, respectively, over the TWNJ path, which is the longest of the two Internet paths. Here, the gap distributions are similar to those measured on the testbed. The intra-probe gap distributions on the NYNJ path are also similar to those measured on the testbed paths. These results, therefore, show that the compound probe arrive at dst over the Internet paths with a zero-dispersion gap and can measure the end-link capacities with similar accuracy to that achieved on the testbed paths.

VI. Conclusions

We presented an analytical model to determine the packet sizes in the packet-pair structure for the measurement of end-link capacity over a network path. The model is derived by considering the heterogeneous link capacities and cross-traffic load of the path to ensure a zero-dispersion gap in the packet pair for accurate end-link capacity measurement. We numerically evaluated the model using different path configurations and cross-traffic loads. We also presented experimental results of end-link capacity measurements on a controlled testbed and in the Internet. The outcomes of the numerical evaluations verify the analytical model. The experiment results show that high measurement accuracy can be achieved, irrespective of link heterogeneity and cross-traffic load of a path, when suitable packet sizes are used in the packet-pair structure. Our experiments also show that the proposed model is practical.

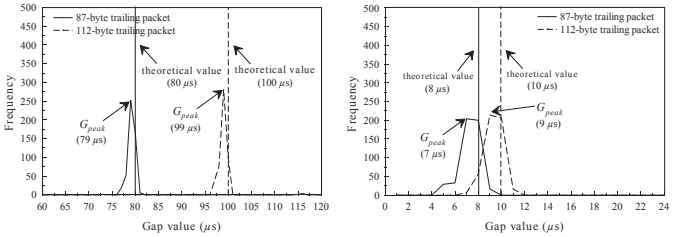

(a) TWNJ-10 (b) TWNJ-100

Fig. 7. Distributions of intra-probe gaps measured at dst over the TWNJ path with (a) 10-Mb/s and (b) 100-Mb/s end links.

Acknowledgements

We would like to thank Frank Aversa (NJIT), Ziqian Dong (NYIT), and Chuan-bi Lin (CYUT) for allowing us access to their networks.

References

[1] R. Carter and M. Crovella, "Measuring bottleneck link speed in packet switched networks," *Performance Evaluation*, vol. 27 and 28, pp. 297–318, 1996.
[2] K. Lai and M. Baker, "Measuring link bandwidths using a deterministic model of packet delay," in *Proc. of ACM SIGCOMM*, Stockholm, Sweden, 2000, pp. 283–294.
[3] C. Dovrolis, P. Ramanathan, and D. Moore, "Packet dispersion techniques and capacity estimation," *IEEE ToN*, vol. 12, no. 6, pp. 963–977, 2004.
[4] R. Kapoor, L. Chen, L. Lao, M. Gerla, and M. Sanadidi, "CapProbe: A simple and accurate capacity estimation technique," in *Proc. of ACM SIGCOMM*, OR, USA, 2004, pp. 67–78.
[5] K. Harfoush, A. Bestavros, and J. Bayers, "Measuring capacity bandwidth of targeted path segments," *IEEE ToN*, vol. 17, no. 1, pp. 80–92, 2009.
[6] K. Salehin and R. Rojas-Cessa, "A combined methodology for measurement of available bandwidth and link capacity in wired packet networks," *IET Communications*, vol. 4, no. 2, pp. 240–252, 2010.
[7] ——, "Active scheme to measure throughput of wireless access link in hybrid wired-wireless network," *IEEE Wireless Communications Letters*, vol. PP, no. 99, pp. 1–4, 2012.
[8] ——, "Scheme to measure relative clock skew of two Internet hosts based on end-link capacity," *IET Electronics Letters*, vol. 48, no. 20, pp. 1282–1284, 2012.
[9] R. Mandeville and J. Perser. RFC 2889 - Benchmarking methodology for LAN switching devices. [Online]. Available: http://www.ietf.org/rfc/rfc2889.txt.
[10] D. Bovet and M. Cesati, *Understanding the Linux Kernel, ch. 5*. CA, USA: O'Reilly, 2001.
[11] Wireshark. [Online]. Available: http://www.wireshark.org/.
[12] R. Prasad, M. Jain, and C. Dovrolis, "Effects of interrupt coalescence on network measurements," in *Proc. of PAM*, France, 2004, pp. 247–256.
[13] G. Jin and B. Tierney, "System capability effects on algorithms for network bandwidth measurements," in *Proc. of ACM IMC, 27-29*, FL, USA, 2003, pp. 27–83.